Towards the Optimal Pattern of Joint Beamforming, User Scheduling and Power Allocation in a multi-RAT Network

Jörg von Mankowski*, Hansini Vijayaraghavan*, Alberto Martinez Alba*, Leonardo Goratti†, Wolfgang Kellerer*
*Chair of Communication Networks, Technical University of Munich, Germany.
{joerg.von.mankowski, hansini.vijayaraghavan, alberto.martinez-alba, wolfgang.kellerer}@tum.de
†Zodiac Inflight Innovations, Wessling, Germany
leonardo.goratti@zii.aero

***Abstract*—Multiple solutions for the coexistence of different radio access technologies operating in the same frequency band have been proposed for 5G and WiFi. Most solutions based on spatial division just consider a small amount of radio access points, one link direction, and/or a single radio access technology. As a consequence, the performance of these solutions on realistic wireless network deployments may be poor and difficult to estimate. This paper investigates the serving of multiple users by multiple radio access technologies with the objective of minimizing the interference among network nodes. This is done by jointly optimizing the beams and link directions as well as the transmission powers, so as to ensure fair and near-optimal throughput allocation over time. For this purpose, a generalized beam-gain model for small-scale antenna arrays is proposed. We evaluate our proposed solution for realistic network scenarios in order to show its effectiveness.**

***Index Terms*—Beamforming, Multi-Technology Coexistence, 5G-NRU, WiFi-6**

I. Introduction

The next generation of networks are envisioned to leverage Multi-Radio Access Technology (Multi-RAT) to satisfy the growing demand for traffic, provide support for users of heterogeneous technologies, and increase the reliability of services. A typical Multi-RAT Network consists of heterogeneous radio channel access technologies which interfere with one another. This interference can be detrimental for high data rate networks, especially with the expected hundredfold increase in data rates in the next generation mobile networks [1]. Moreover, with energy efficiency gaining in importance, the interference becomes a major impediment since it leads to packet losses resulting in re-transmissions. This also causes the network to fall short of the sub-ms delay requirement of 6G networks [2]. To reduce the interference between the technologies, different coexistence concepts [3] such as frequency domain (FD) and time domain (TD) division of the channel, as seen in Carrier Sensing Adaptive Transmission (CSAT) and Listen Before Talk (LBT), have been developed. Apart from these, concepts for optimal power allocation and successive interference cancellation (SIC) are proposed to mitigate interference. One promising approach is spatial division multiple access (SDMA) which offers spatial multiplexing implemented by solutions including Multiple Input Multiple Output (MIMO), Multi User MIMO (MU-MIMO) and beam forming (BF) or even cooperative solutions such as Cooperative Multiple Input Multiple Output (Co-MIMO).

BF is accomplished with the techniques of digital BF, analog BF, and hybrid BF. In digital BF, all signals for the antenna elements are generated digitally to form the beam of the antenna array, whereas in analog BF, one digital signal is modified with an analog circuit per antenna element to form a beam. In hybrid BF [4], both approaches are combined to find an optimum in installation space and power consumption. However, most of the research is focused on generating the optimal signal at each antenna of the antenna array. In contrast, we abstract the antenna array by focusing on the beam angle.

Apart from the beams, other wireless resources can also be allocated efficiently to optimize the network. In resource allocation, transmission power is an important factor as it influences the Signal to Interference Noise Ratio (SINR) for the receiver as well influencing the interference for other network nodes. The SINR has a direct effect on the achievable data rate. Another component of resource allocation that has to be taken into account is the link transmission direction. Scheduling the radio client (RCL) for uplink transmission and optimally allocating downlink transmissions to satisfy latency constraints is vital. For an optimal network configuration, all three variables influence the SINR of the link and consequently, the link properties (e.g. achievable capacity, delay, etc.) and should, therefore, be jointly optimized.

A. Related Work

The authors in [5] apply machine learning to decide the optimal beam to communicate with one RCL based on the location information of the user. However, the system does not try to optimize for multiple RCLs or even multiple radio access points (RAPs). Optimally allocating multiple RCLs in one cluster to serve them over Orthogonal Frequency-Division Multiple Access (OFDMA) is described in [6]. The communication is based on one antenna array shared by 5G and WiFi. The beams are calculated by optimizing the precoding matrix. Although multiple technologies are used, they

originate from the same antenna, relaxing the problem of interference. Overlapping beams which could cause interference are tackled in [7]. They propose the usage of a narrow beam to improve the SINR. Furthermore, they solve the interference by assigning different frequencies to spatially overlapping beams. This solution is also described in [8]. However, they do not consider the interference at the corners of the sectorization of the physical space. By avoiding interference using frequency division of overlapping beams, they reduce the maximum theoretical spectral efficiency by 50%. This inefficiency is avoided in [9]. They compare different user clustering algorithms resulting in spectrum sharing. However, these would yield unfair rate distributions, as the beam allocation over time does not compensate for the cluster density. All these concerns are addressed in [10]. However, the described optimization problem avoids optimizing uplink and downlink together for networks containing more than two RAPs. In most of these papers, the optimization for the beam is based on precoding matrices.

B. Contribution

In this paper, we propose an abstract model for beamforming antenna array networks, independent of underlying beamforming technology. In addition, we combine our model with a proposed approach to improve performance in a heterogeneous network with interfering 5G and WiFi links. This is accomplished by formulating a resource allocation optimization problem with the objective of maximizing the average network sum throughput while maintaining rate fairness among users over the time slots and minimizing the number of users left unserved. We then solve this problem using multiple meta-heuristic and approximate solvers. As a result of this optimization, we allocate the optimal beam angle of the RAPs, transmission power, and uplink/downlink transmission slots of all devices for multiple time instances for a fixed time period. We then evaluate the solutions for different network topologies and system parameters.

C. Organization

The rest of the paper is organized as follows. Section II introduces the system model considered. The optimization problem is described in Section III. Section IV details the solution methods to this optimization problem and the methods are evaluated in Section V. Finally, Section VI concludes the paper.

II. System Model

The following conventions apply: $\vec{v}$ denotes a vector, capital bold letters ($\mathbf{M}$) represent matrices, and $\cdot$ is the element-wise multiplication between two vectors or matrices.

A. Wireless devices

In this paper, a device is referred to as a radio transmission point (RTP). It can be either a 5G-NR-U or a WiFi6 device. We further distinguish between two classes of RTPs, the radio access point (RAP) and the radio client (RCL). The connection

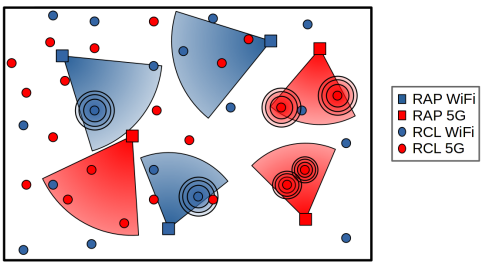

Fig. 1. Scenario Overview

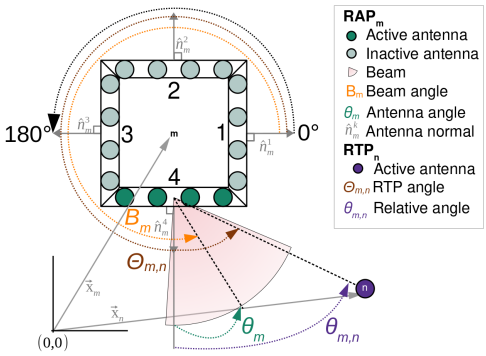

Fig. 2. Antenna Description

between an RCL and the associated RAP is defined as link i. α_u contains the RAP associated and u_i contains the RCL of link i. α_u and u_i form vectors $\vec{\alpha}, \vec{u}$. Multiple RCLs of $\vec{u}$ connect to one RAP of $\vec{\alpha}$ of the same technology based on shortest distance. While RAPs communicate directional by BF, RCLs communicate omnidirectional. In consequence, the transmission gain between two RTPs m and n depend on the RAP's beam B and their positions $\vec{x}_m, \vec{x}_n$, for down-link (DL) and up-link (UL). An overview of the system is given in Fig. 1.

B. Antenna configuration

Multi-antenna arrays require a large installation space. This is not available in the majority of the application scenarios described in Sec. II-D. Therefore, we focus on small antenna arrays. Every RAP is equipped with 4 antenna arrays with each antenna array having 4 antenna elements each, as shown in Fig. 2. Instead of using MU-MIMO or BF to allocate a subset of the antennas per RCL, the entire antenna array is used to connect multiple RCLs using OFDMA. This is achieved by generating a wider beam compared to standard BF. This results in a beam width of approximately $47°$ with an antenna spacing of $\frac{\lambda}{2}$ where the beam gain is 1. The angle between the antenna arrays is $90°$. The beam angle of the RAP is denoted by B. The antenna array with the smallest difference between its normal and beam angle is active. The antenna angle θ_m is calculated by (1)

$$\theta_m = B_m - \arg(\hat{n}_m^k) \ , \tag{1}$$

with $\hat{n}_m^k$ being the antenna normal and $k = \left\lceil \frac{B_m - \frac{\pi}{4}}{2\pi} \right\rceil$. The angle between two RTPs, the RTP angle $\Theta_{m,n}$, is calculated by

$$\Theta_{m,n} = \arg(\vec{x}_m - \vec{x}_n) \ . \tag{2}$$

The angle relative to the active antenna, the relative angle $\theta_{m,n}$, is calculated by

$$\theta_{m,n} = \Theta_{m,n} - \arg(\hat{n}_m^k) \ . \tag{3}$$

For simplicity, we assume that RTPs positioned behind an active RAP antenna receive a gain of 0. Otherwise the gain between two RTPs (m and n) is calculated by the following equations.

$$g_{m,n} = \begin{cases} g(\theta_m, \theta_{m,n}) g(\theta_m, \theta_{m,n}) & \text{if } n, m \text{ are RAPs} \\ 1 & \text{if } n, m \text{ are RCLs} \\ g(\theta_m, \theta_{m,n}) & \text{if } m \text{ is RAP, } n \text{ is RCL} \\ g(\theta_n, \theta_{n,m}) & \text{if } n \text{ is RAP, } m \text{ is RCL} \end{cases} \tag{4}$$

$$g(\theta_m, \theta_{m,n}) = \left| \frac{\sin(2\pi[\sin(\theta_{m,n}) - \sin(\theta_m)])}{4\sin(0.5\pi[\sin(\theta_{m,n}) - \sin(\theta_m)])} \cos(\theta_{m,n}) \right| \tag{5}$$

C. Link and Coverage

RAPs can be configured as either DL or UL for a time slot. The link direction of the RCLs is given by the configuration of the RAP it is associated to. Not all RCLs can be covered simultaneously by their corresponding RAP beam. Therefore, the beam angle needs to be adapted over time, so that every RCL is covered. To achieve this, we divide the simulation into slots of 1 ms. The minimum slot size for 5G, disregarding 5G-URLLC, is 1 ms and the variable frame duration of WiFi allows a channel occupancy of less than 1 ms in every modulation scheme. This motivates the slot size being 1 ms. The maximum time an RCL can be out of coverage is 400 ms (5G-NR-U for timer T300 [11]) and < 1 s (WiFi 6) before resulting in a disconnection. In addition, 5G-NR-U can exhibit a maximum channel occupancy time of up to 8 ms [11] requiring a movement of the beam at least every 8 ms. We assume that all RTPs operate at the same frequency. Therefore, a user link (DL, UL) will experience interference from every RAP operating in DL and RCLs in UL except from the RCLs connected to the same RAP.

D. Scenarios

In order to evaluate our approach, we focus on multiple realistic scenarios which vary in radio client and access point count, offering a spatial diversity in user positions and different channels. The scenario-specific channels are based on large scale path loss models described by

$$PL_{Channel}(d) = PL_0 + n_{ch} \cdot 10\log_{10}(d) + X_{Channel}[dB] \ , \tag{6}$$

with $PL_0 = 20\log_{10}4\pi f_c/C$ being the frequency dependent component, C is the speed of light, n_{ch} denotes the channel specific distance exponent, and $X_{Channel}$ is a channel specific random variable following the specified distribution

TABLE I
SCENARIO PARAMETERS

Parameter	Bus	Train	Aircraft	Office	Outdoor
RAP WiFi+5G	1+1	1+1	3+3/4+4	4+2	2+2
RCL WiFi+5G	30+30	37+37	167+167	60+30	50+50
Cover area m^2	35	71.25	272.5	1250	20000
n_{ch}	1.779	1.8	2.65	1.8	2.0
Distribution	Normal	Normal	Rician	Normal	Lognormal
Parameter 1	μ=0	μ=0	s=0.465	μ=0	μ=0
Parameter 2	σ=10.22	σ=2.3	σ=0.150	σ=1.65	σ=4.1

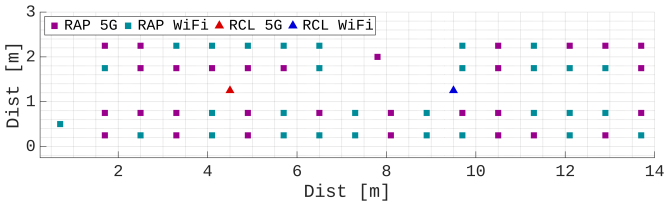

Fig. 3. Bus Topology

of Table I. We assume a center frequency $f_c = 2.4$ GHz and a signal bandwidth $BW = 20$ MHz for our simulations. We consider transportation scenarios since this is a common application for a multi-technology network. Many user devices are equipped with only a certain specific technology, like user laptops having only WiFi capability and not 5G. For transportation scenarios, the technology for the RCLs is varied among multiple simulation runs. In the office and outdoor scenarios the location of the RCLs also varies. The position and technology of the RAPs are maintained.

1) Bus: This scenario models a typical configuration that could be found in an intercity bus service. The model was based on the dimensions of a Travego RHD-L. Fig. 3 displays the RTP distribution. The channel is modeled by (6) and based on the work in [12], with the corresponding parameters from Table I.

2) Train: The train configuration is based on a German high-speed train seat wagon of the ICE T. Fig. 4 displays the RTP distribution. The channel is modeled by (6) based on the results in [13], with the corresponding parameters from Table I.

3) Aircraft and Aircraft+2: The aircraft and aircraft+2 configurations are based on an Airbus A340-300. Fig. 5 displays the RTP distribution for aircraft. Compared to the aircraft model, two additional RAPs are installed (at 24.2 m) in the aircraft+2 model. The channel is modeled by (6) based on the results in [14].

4) Office: For the office, the distribution of 5G:WiFi RCLs and RAPs is 1:2. Fig. 6 displays one exemplary spatial distribution of RTPs. The channel includes the effects of walls on the pathloss as described in (7). The channel is based on the work in [15]:

$$PL = PL_0 + 18\log_{10}(d) + 8 \cdot \lceil d/10 \rceil + X_{Office} \ , \tag{7}$$

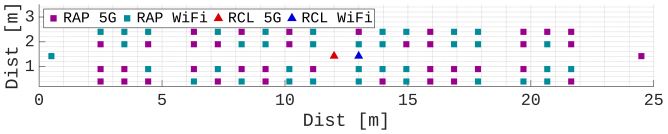

Fig. 4. Train Topology

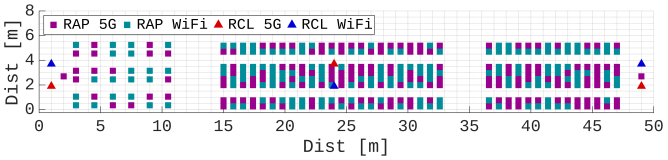

Fig. 5. Aircraft Topology

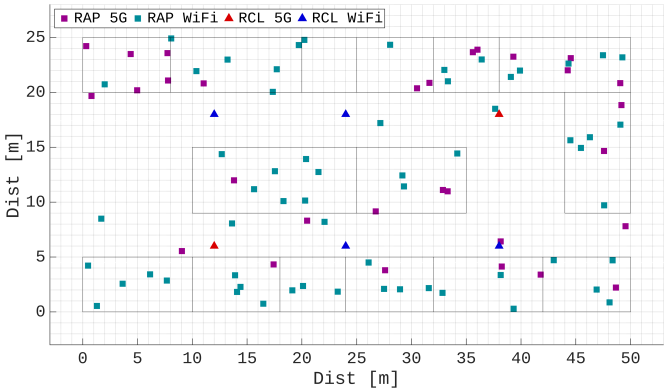

Fig. 6. Office Topology

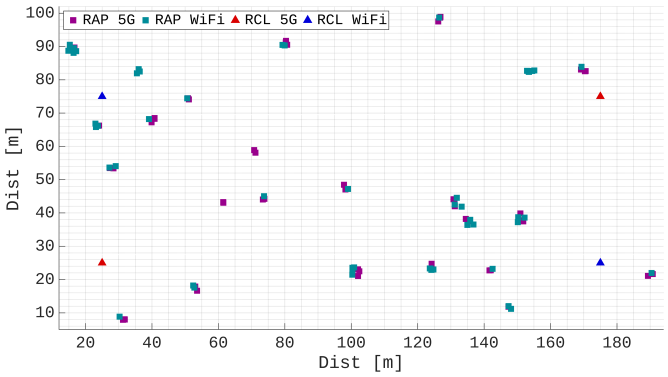

Fig. 7. Outdoor Cluster Topology

with X_{Office} being a normal distributed random variable (r.v.) with a mean $\mu = 0$ and standard deviation $\sigma = 1.65$.

5) Outdoor Cluster, Outdoor Random: The outdoor scenario can be differentiated into a cluster type and a random type. In the cluster type, RCLs appear in groups as depicted in Fig. 7 whereas, in the random type, RCLs are randomly distributed over the area. The channel is based on the work of [16] and described in (6). Furthermore, we assume that during the optimization instance the coherence time of all channels is 40 ms [17] since we consider a low mobility scenario with a user speed << 0.36 m/s.

III. Optimization Problem Formulation

In this section, we describe the problem formulation for maximizing the throughput of all RCLs, considering user fairness, for DL and UL, and minimizing the service waiting time for RCLs. Solving this problem results in the optimal values for the beam angle $\vec{B}$, the transmission powers for the RTPs $\vec{P}$, the link configuration $\vec{L}$ and an optimal sequence of these parameters $\mathbf{B} = [\vec{B}_1, \vec{B}_2, ..., \vec{B}_T]$ over a time period T. We similarly define $\mathbf{P}$ and $\mathbf{L}$ as the sequences of transmission powers and link configurations, respectively. To achieve the optimal sequence over time we divide the time into a finite amount of slots $T = 40$. In addition, we do not optimize data rate on its own, as it might lead to an unfair distribution, but we apply a proportional fair utility function as described by [18].

This allows us to divide the problem into a one-shot optimization for each slot t and a function that penalizes solutions found in previous slots. Both problems are combined in (8) by calculating the utility function, dependent on the throughput, referred to as UF:

$$UF(t) = \sum_{i=1}^{I} \psi \frac{r_i^{DL}(t)}{r_i^{HDL}(t)} + (1-\psi)\frac{r_i^{UL}(t)}{r_i^{HUL}(t)} \ , \qquad (8)$$

with ψ being a weight factor for the DL-UL-ratio, r_i^{DL} the current DL-rate, r_i^{UL} the current UL-rate, r_i^{HDL} the DL and r_i^{HUL} the UL penalty factor of link i. The value of ψ can be straightforwardly obtained by exhaustive search to find the value resulting in an UL:DL ratio of ca. 1:6. This ratio depicts the average ratio of typical asymmetric downlink to uplink traffic in the considered network scenarios [19]. Variables r_i^{DL} and r_i^{UL} are the current rates of the link i between the RAP and the associated RCL in the DL and UL, respectively, including a bandwidth correction for the number of RCLs, N_i, connected to the same RAP. The rate r_i^{xL} is calculated from the spectral efficiency g, dependent on SINR, as:

$$r_i^{xL} = g(\eta_i)\frac{BW}{N_i}.$$

The SINR to spectral efficiency mappings for 5G and WiFi are described in [20] and [21] respectively. The penalty factors r_i^{HDL}, r_i^{HUL} are calculated by:

$$r_i^{HxL}(t) = \begin{cases} 1 & \text{if } t = 1 \\ \frac{r_i^{HxL}(t-1)t}{t+1} + \frac{r_i^{xL}(t-1)}{t+1} \ , r_i^{HxL}(1) = 1 & \text{if } t > 1 \end{cases}. \qquad (9)$$

The value of r_i^{HxL} increases each time the link has been served. By dividing solutions, that benefit the same link, by their history, the link is penalized and other solutions benefiting different links can be found by the solvers. This ensures that more RCLs are served and that the rate is distributed more fairly among the users, independent of the channel impairments while at the same time the terms r^{HDL} and r^{HUL} ensure penalizing DL and UL separately.

The SINR η_i is calculated as:

$$\eta_i = \frac{g_i \cdot h_i \cdot P_i}{\sum_{j=1}^{J_i} g_{m_i,n_j} \cdot h_{m_i,n_j} \cdot P_j} \ , \tag{10}$$

with $g_i = g_{u_i,\alpha_{u_i}}$ being the gain, $h_i = h_{u_i,\alpha_{u_i}}$ the channel effect, and $P_i = L_{\alpha_{u_i}} \cdot P_{\alpha_{u_i}} + (1 - L_{\alpha_{u_i}}) \cdot P_{u_i}$, the transmission power in the link i and J_i being all links except links associated to the same α_{u_i}, and

$$m_i = (1 - L_{\alpha_{u_i}}) \cdot \alpha_{u_i} + L_{\alpha_{u_i}} \cdot u_i,$$
$$n_j = L_{\alpha_{u_j}} \cdot \alpha_{u_j} + (1 - L_{\alpha_{u_j}}) \cdot u_j.$$

That is, the values of m_i and n_j depend on whether the transmission of the link is in DL or UL. For the sake of simplicity, we omit the link subscript in the following formulas. The gain $g_{m,n}$ is calculated by (4) and the channel $h_{m,n}$ by

$$h_{m,n} = PL_{Channel}(||\vec{x}_m - \vec{x}_n||) \ , \tag{11}$$

where $PL_{Channel}$ is described by (6) and (7). The objective of the optimization is to maximize the utility function UF. Hence, the optimization problem is formulated as:

$$\max_{\mathbf{B},\mathbf{P},\mathbf{L}} UF(t) \tag{12}$$
$$L_{\alpha,t} \in \{0,1\} \qquad B_{\alpha,t} \in [0, 2\pi]$$
$$P_{\alpha,t} \in [-40,-10] \qquad P_{u,t} \in [-40,-10]$$

with $L_{\alpha,t}$ = 1 representing DL, $L_{\alpha,t}$ = 0 the UL, $P_{\alpha,t}$ the the transmission power of RAP, and $P_{u,t}$ the transmission power of RCL in dBW. The power bounds are the maximum allowed transmission power in Europe of 100 mW and the minimum configurable transmission power for WiFi of 0.1 mW.

IV. Solution Methods

The optimization problem described in Sec. III is a Mixed Integer Nonlinear Program (MINLP) since it has integer $\mathbf{L}$ and real values $\mathbf{B}$ and $\mathbf{P}$ and the influence of these on the utility function over time is nonlinear. Since, in general, MINLPs are NP-Hard and thus difficult to tackle, we use multiple metaheuristics and approximate methods to solve the problem and compare the results. The methods that we evaluate in this work are: simulated annealing (SA) [22], genetic algorithm (GA) [23], particle swarm (PW) [24], pattern search (PT) [25], interior point (IP) [26], and surrogate (SG) [27]. The integer constraint is relaxed for solvers that do not accept integer variables. The solution is then rounded to the nearest integer.

SA imitates the heating of a material followed by the steady decrease of temperature reducing defects, thereby, minimizing the energy of the system. Similarly, the solver generates potential solutions at each temperature state, accepting only good solutions and repeating this process until convergence.

GA is a metaheuristic that models the theory of natural selection where the fittest candidate solutions of each generation are selected to reproduce and generate the candidates of the next generation.

The concept of PW is based on a swarm of candidate solutions that move through a region in steps based on a formula depending on their position and velocity . The algorithm evaluates the utility function for each particle and step. Depending on the result, the movement is adjusted for each particle until convergence.

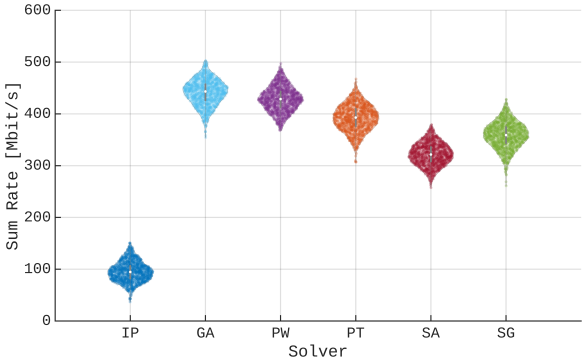

Fig. 8. Comparison of sum rate for different solvers for the Outdoor Random topology

The pattern in PT refers to a set of candidate solutions where the utility function is evaluated. Depending on whether a better solution is found or not, the mesh or search space for the next pattern is expanded or contracted.

IP is a gradient-based nonlinear programming solver. It uses the interior-point algorithm to solve a constrained minimization wherein it solves a sequence of approximate optimization problems.

SG is recommended for expensive objective functions with nonlinear inequality constraints and integer constraints. To solve the problem, the optimizer evaluates the surrogate, which is the approximation of the objective function, on multiple candidate solutions and takes the best values as an approximation of the optimal values of the original objective function. It is to be noted that, in this paper, SG is terminated after a maximum of 230 function evaluations. This is comparable with the average function evaluations of the other solvers when their termination is determined by an objective function tolerance of 10^{-2} over a maximum of 50 stall iterations.

V. Evaluations and Discussions

The optimization problem is solved using the solvers described in Sec. IV and is extensively evaluated with simulations. The simulations are performed for varying network topologies and for different power and beam configurations. The results of 1000 simulations for each evaluation are presented in this section.

The optimization problem for the Outdoor Random scenario is solved and the resulting network sum rate is shown in Fig. 8. Additional network Key Performance Indicators (KPIs) are described in Table II. From the table, we observe that IP performs the worst in terms of sum rate, the Jain fairness indicators [28] in DL and UL, and the number of unserved RCLs. This is due to the non-continuous nature of the objective function and its gradients. Due to its poor performance, we exclude this solver for the following analysis. GA yields the

TABLE II
KPIs FOR OUTDOOR RANDOM SCENARIO

	IP	GA	PW	PT	SA	SG
DL [Mbit/s]	63.87	343.04	310.35	284.87	255.71	309.49
UL [Mbit/s]	31.42	98.112	118.34	107.19	66.034	49.225
Achieved ψ	67%	77.8%	72.4%	72.7%	79.5%	86.3%
unserved RCL	49	17	17	19	18	19
Jain DL	0.374	0.704	0.656	0.658	0.634	0.660
Jain UL	0.225	0.403	0.418	0.446	0.466	0.434
SideLobeUse	20.1%	22.3%	22.9%	21.5%	24.2%	24.8%

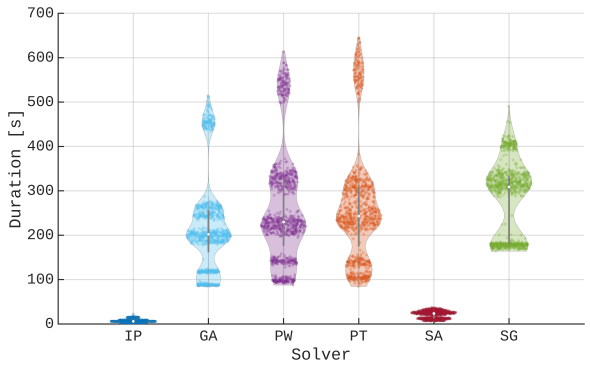

Fig. 9. Comparison of run time in CPU time for different solvers for the Outdoor Random topology

TABLE III
HLM RESULTS

Name	Mean Difference	SE	Lower	Upper
GA-SA	200.19	2.662	194.97	205.41
PW-SA	242.08	2.662	236.86	247.3
PT-SA	247.37	2.662	242.15	252.59
SG-SA	257.26	2.662	252.04	262.48

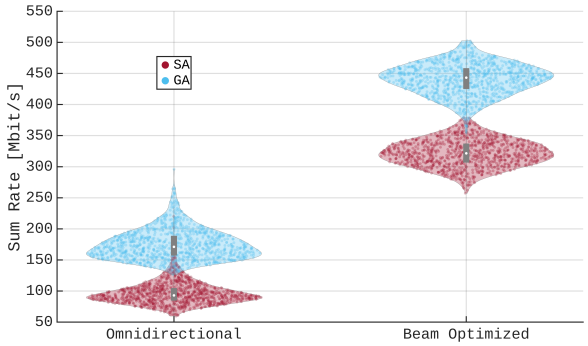

Fig. 10. Comparison of sum rate for varying beam configurations for SA and GA

highest sum rate, while also serving the maximum amount of users and still approaching ψ closely. For all these reasons we continue further analysis with this optimizer. The SideLobeUse denotes the percentage of data transmitted over the side lobes. Interestingly, by optimizing for the data rate ca. 1/5th of the transmission for all optimizers is over side lobes which is undesirable in other works, because of the expected interference. However, our approach includes this effect in the rate calculation and is, therefore, able to benefit from this type of transmission.

To analyze the time to solve for the different optimization algorithms, we measure the actual time a CPU core spends on solving the problem. This should reduce the variance between different multi-core systems. However, the distribution of the duration for each solver still indicates a hardware-dependent component as seen in Fig. 9 which shows the duration for each solver for the outdoor random scenario. To provide more insight on the calculation duration we computed a Hierarchical Linear Model (HLM) with Duration as criterion and Solver as the predictor variable. The model uses SA as the reference and creates 4 variables representing the other Solvers except for IP. We control for the co-variate Worker, as different computers were used to generate the results and hence likely to confound the duration. The model is described by (13).

$$Duration_{i,m} = \beta_0 + \beta_1(GA - SA) + \beta_2(PW - SA) + \beta_3(PT - SA) + \beta_4(SG - SA) + b_{0,m} + \epsilon_{i,m} \quad (13)$$

where, $Duration_{i,m}$ is the criterion of observation i, for the grouping variable Worker represented by m. Here, $i \in \{1, 2, ..., 1000\}$ and $m \in \{1, 2, ...8\}$. β_j, $j \in \{1, 2, 3, 4\}$ are the fixed effect coefficients, β_0 is the intercept, and $b_{0,m}$ is the random effect of the grouping variable, and $\epsilon_{i,m}$ is the observation error for i. The effect of different computers is confirmed by a 9376 point smaller AIC value for a model including Worker compared to a model solely based on Optimizer. The AIC is an indicator of how well a model fits the underlying data, with smaller AIC values indicating a better fit. The variance in the data that can be explained by this model is R^2 = 85%. Table III shows the results of this model and the difference in mean values and the corresponding 95% confidence intervals. We can infer from Table III, that SA is the fastest optimizer as all mean differences are significantly greater than 0. Hence, for the following evaluations, we use SA to compare with GA.

Fig. 10 shows a comparison between omnidirectional communication and our proposed beam-optimized system. While both scenarios use the same amount of RAPs, the beam-optimized network is able to increase the sum rate by a factor of 2.5. As expected, SA performs worse.

Fig. 11 shows the optimized sum rate for various scenarios. In general, GA performs better than SA. However, when increasing the amount of RAPs to increase the throughput for high-density environments such as an aircraft, SA is not able to make use of the 2 additional RAPs in the aircraft+2 scenario. Although GA is able to leverage the two additional RAPs for the sum throughput the spectral efficiency decreases from 6.197 bits/s/Hz to 4.915 bits/s/Hz.

In all scenarios except the outdoor scenario, all RCLs are served with GA. The users left unserved in Outdoor Random are due to the harsh channel conditions and could not have been served even with a directly allocated beam.

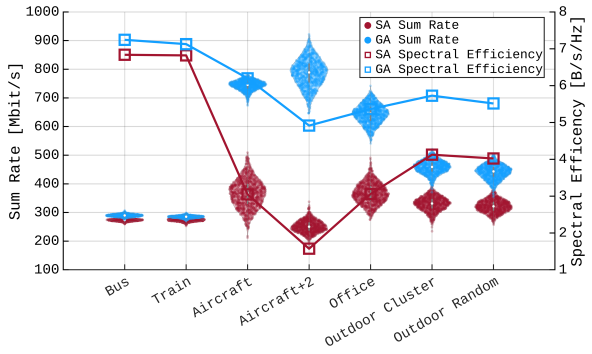

Fig. 11. Comparison of sum rate and spectral efficiency for different scenarios for SA and GA

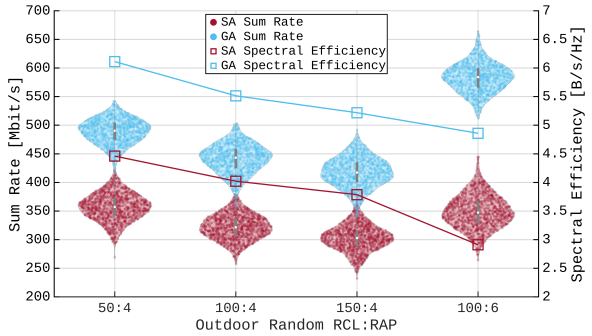

Fig. 12. Comparison of sum rate and spectral efficiency for different RCL to RAP ratio for SA and GA

The clustering of users, compared to a random distribution, yields better results. This is, in part, due to the reduced space that needs to be covered by the beams.

The results for varying RCL to RAP ratio in the Outdoor Random scenario are shown in Fig. 12. Increasing the number of RCLs for the same number of RAPs decreases the sum rate and spectral efficiency due to more transmitting RCLs causing interference and the larger area to be covered by the RAPs. However, by increasing the number of RAPs, the optimizer can leverage the additional capacity and increase the sum rate at the cost of a reduced spectral efficiency. Here, GA performs much better than SA.

An additional comparison is made in the Outdoor Random scenario between the power-optimized network and networks with fixed transmission powers while still optimizing for the other variables. The results of this comparison for GA are depicted in Fig. 13. The powers of the RCLs are fixed to the values in the figure and the powers of all RAPs are fixed to 100 mW. Contrary to expectations, fixing the RCL transmission power to 100 mW increases the throughput in DL and decreases the throughput in UL compared to a power of 20 mW. This is due to the fact that, by increasing the power, more users are being served by an RAP in fewer slots, resulting in more slots being allocated to the DL. This is shown in Table IV.

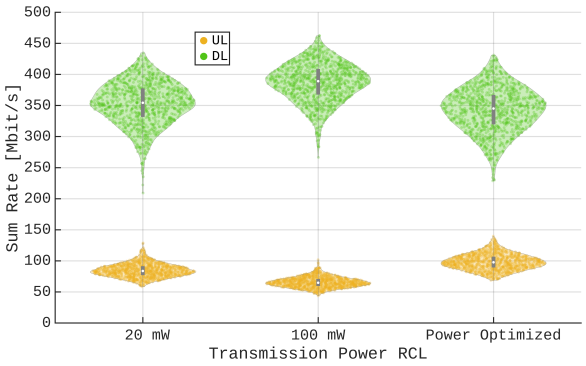

Fig. 13. Comparison of DL and UL sum rate for varying transmission power configurations

TABLE IV
PERCENTAGE OF SLOTS ALLOCATED TO DL

RAP	1	2	3	4
20mW	88.7%	88.6%	82.9%	81.4%
100mW	89.9%	89.9%	87.6%	86.9%

VI. CONCLUSION

In this paper, we propose a beam-gain model based only on beam angle and eliminating precoding matrices. In addition, the considered antenna array allows for small installation spaces, crucial for most of the application scenarios described in this work. We also propose a resource allocation approach for heterogeneous networks and evaluate it in detail with multiple metaheuristics. The results verify that only a minimum amount of RAPs are needed to cover most transportation scenarios with 5G and WiFi. This is accomplished by optimizing for the transmission power, the beam angle, and the link direction of all RTPs, while keeping the number of unserved users to a minimum. We also show, that increasing the number of RAPs can benefit the network throughput but reduces the spectral efficiency. In addition, we show that our approach is able to increase the network throughput compared to the baseline. We also conclude that fixing the transmission power influences the sum throughput minimally, as opposed to its influence on the throughput distribution between UL and DL.

ACKNOWLEDGMENT

The authors thank Yannik Hilla (Ludwig-Maximilians-Universität in Munich) for his help with the HLM and for comments on the manuscript. This work was supported by Munich Aerospace e.V..

REFERENCES

[1] T. Taleb, R. L. Aguiar, I. Grida Ben Yahia, B. Chatras, G. Christensen, U. Chunduri, A. Clemm, X. Costa, L. Dong, J. Elmirghani *et al.*, "White paper on 6G networking," 6G Research Visions no. 6, University of Oulu, White paper, 2020.

[2] C. J. Bernardos and M. A. Uusitalo, "European vision for the 6g network ecosystem," Jun. 2021. [Online]. Available: https://doi.org/10.5281/zenodo.5007671

[3] G. Naik, J.-M. Park, J. Ashdown, and W. Lehr, "Next generation wi-fi and 5g nr-u in the 6 ghz bands: Opportunities and challenges," *IEEE Access*, vol. 8, pp. 153 027–153 056, 2020.

[4] I. Ahmed, H. Khammari, A. Shahid, A. Musa, K. S. Kim, E. De Poorter, and I. Moerman, "A survey on hybrid beamforming techniques in 5g: Architecture and system model perspectives," *IEEE Communications Surveys Tutorials*, vol. 20, no. 4, pp. 3060–3097, 2018.

[5] D. Wu, Y. Zeng, S. Jin, and R. Zhang, "Environment-aware and training-free beam alignment for mmwave massive mimo via channel knowledge map," IEEE, pp. 1–7, 2021.

[6] Q. Chen, X. Xu, and H. Jiang, "Spatial multiplexing based nr-u and wifi coexistence in unlicensed spectrum," in *2019 IEEE 90th Vehicular Technology Conference (VTC2019-Fall)*. IEEE, 2019, pp. 1–5.

[7] Y. A. Abohamra, M. R. Soleymani, and Y. R. Shayan, "Using beamforming for dense frequency reuse in 5g," *IEEE Access*, vol. 7, pp. 9181–9190, 2019.

[8] L. A. Ferhi, K. Sethom, and F. Choubani, "Multi-carrier 3d beamforming for 5g ultra-dense cellular networks," in *2018 International Conference on Advanced Systems and Electric Technologies (IC_ASET)*. IEEE, 2018, pp. 221–226.

[9] F. Costa Neto and T. Ferreira Maciel, "Sdma grouping based on unsupervised learning for multi-user mimo systems," *Journal of Communication and Information Systems*, vol. 35, no. 1, pp. 124–132, May 2020.

[10] M.-L. Ku, L.-C. Wang, and Y.-L. Liu, "Joint antenna beamforming, multiuser scheduling, and power allocation for hierarchical cellular systems," *IEEE Journal on Selected Areas in Communications*, vol. 33, no. 5, pp. 896–909, 2014.

[11] 3GPP, "TR 28.801 V15.1.0 (2018-01); Technical Report; Study on management and orchestration of network slicing for next generation network (Release 15)," 3rd Generation Partnership Project (3GPP), Tech. Rep., 2018.

[12] L. Azpilicueta, P. L. Iturri, E. Aguirre, *et al.*, "Characterization of wireless channel impact on wireless sensor network performance in public transportation buses," *IEEE Transactions on Intelligent Transportation Systems*, vol. 16, no. 6, pp. 3280–3293, 2015.

[13] W. Dong, G. Liu, L. Yu, H. Ding, and J. Zhang, "Channel properties of indoor part for high-speed train based on wideband channel measurement," in *2010 5th International ICST Conference on Communications and Networking in China*. IEEE, 2010, pp. 1–4.

[14] N. Riera Díaz, J. E. Jiménez Esquitino, O. Franzrahe, T. Eisenberg, P. Veith, and A. Pohl, "IST-2001-37466 WirelessCabin In-Cabin Channel Measurement Performance and Result Report," DLR, Tech. Rep., 2004.

[15] T. Chrysikos, P. Georgakopoulos, I. Oikonomou, S. Kotsopoulos, and D. Zevgolis, "Channel measurement and characterization for a complex industrial and office topology at 2.4 ghz," in *2017 11th International Conference on Software, Knowledge, Information Management and Applications (SKIMA)*. IEEE, 2017, pp. 1–8.

[16] M. Alhammadi, M. Almansoori, I. Tesfu, D. Habte, and I. Ahmed, "Large-scale empirical model for a 2.4 ghz wireless network in an outdoor environment," in *2019 Advances in Science and Engineering Technology International Conferences (ASET)*. IEEE, 2019, pp. 1–4.

[17] D. Tse and P. Viswanath, *The wireless channel*. Cambridge University Press, 2005, p. 10âĂŞ48.

[18] M. Andrews, "Instability of the proportional fair scheduling algorithm for hdr," *IEEE Transactions on Wireless Communications*, vol. 3, no. 5, pp. 1422–1426, 2004.

[19] H. Yomo and S. Hara, "An uplink/downlink asymmetric slot allocation algorithm in cdma/tdd-based wireless multimedia communications systems," in *IEEE 54th Vehicular Technology Conference. VTC Fall 2001. Proceedings (Cat. No. 01CH37211)*, vol. 2. IEEE, 2001, pp. 797–801.

[20] Y. Wang, W. Liu, and L. Fang, "Adaptive modulation and coding technology in 5g system," in *2020 International Wireless Communications and Mobile Computing (IWCMC)*. IEEE, 2020, pp. 159–164.

[21] D. Urban, "The importance of wi-fi 6 technology for delivery of gbps internet service," *SCTE ISBE Cable-Tec Expo*, 2019.

[22] L. Ingber *et al.*, "Adaptive simulated annealing (asa)," *Global optimization C-code, Caltech Alumni Association, Pasadena, CA*, 1993.

[23] D. E. Goldberg, *Genetic Algorithms in Search, Optimization and Machine Learning*, 1st ed. Addison-Wesley Longman Publishing, 1989.

[24] J. Kennedy and R. Eberhart, "Particle swarm optimization," in *Proceedings of ICNN'95-international conference on neural networks*, vol. 4. IEEE, 1995, pp. 1942–1948.

[25] C. Audet and J. E. Dennis Jr, "Analysis of generalized pattern searches," *SIAM Journal on optimization*, vol. 13, no. 3, pp. 889–903, 2002.

[26] R. H. Byrd, J. C. Gilbert, and J. Nocedal, "A trust region method based on interior point techniques for nonlinear programming," *Mathematical programming*, vol. 89, no. 1, pp. 149–185, 2000.

[27] M. J. Powell, "The theory of radial basis function approximation in 1990," *Advances in numerical analysis*, pp. 105–210, 1992.

[28] R. K. Jain, D.-M. W. Chiu, W. R. Hawe *et al.*, "A quantitative measure of fairness and discrimination," *Eastern Research Laboratory, Digital Equipment Corporation, Hudson, MA*, 1984.